Original scientific article
http://dx.doi.org/10.59456/afts.2024.1630.059M

STATE-OF-THE-ART APPLICATION OF THE LOG-PILING METHOD IN THE ROLE OF SHALLOW GROUND IMPROVEMENT FOR LIQUEFACTION MITIGATION

Milev Nikolay[1], Takashi Kiyota[2], Shoei Osawa[2], Atsunori Numata[3]

[1]*University of Architecture, Civil Engineering and Geodesy (UACEG), Department of Geotechnics, Sofia, Bulgaria, e-mail: milev_fte@uacg.bg*
[2]*The University of Tokyo, Institute of Industrial Science, Tokyo, Japan*
[3]*Research Institute of Technology, Tobishima Corporation, Chiba, Japann*

SUMMARY

This research paper focuses on evaluating the log piling technique as a sustainable, cost-effective, and environmentally friendly solution for reducing soil liquefaction risks during earthquakes. Although this method has been used extensively in Japan, mainly aiming for complete soil layer penetration, its economic viability is questionable in cases requiring very deep soil improvements. The study highlights that shallow ground improvement can notably enhance the seismic behavior of the soil-improvement-structure system, as evidenced by the reduced total and penetration settlements caused by liquefaction. The paper presents a methodology for determining the optimal dimensions of the modified ground zone using both small and medium-scale 1-g shaking table tests.

The small-scale tests involve a detailed parametric study, examining variables like improvement width, pile spacing, and the depth-to-thickness ratio of the improved layer. Medium-scale tests, on the other hand, are geared towards identifying the minimum effective pile length. This approach provides a practical guideline for engineers to implement log piling for small residential buildings. Additionally, the paper utilizes finite element method (FEM) effective stress analysis, incorporating a PLAXIS 2D-based constitutive model (PM4Sand) calibrated with laboratory undrained cyclic torsional tests. This model accounts for the changes in effective stress during seismic activities. Finally, the study correlates its numerical findings with the results from the 1-g shaking table experiments, offering a well-rounded perspective on the effectiveness of log piling in mitigating liquefaction risks during seismic events

Key words: *soil liquefaction, log-pile, soil improvement, 1-g shaking table test, numerical study, constitutive model, effective stress analysis*

INTRODUCTION

In recent years, the escalating issue of global warming and climate change has risen to the forefront of societal concerns. One promising avenue for long-term carbon dioxide storage, the primary driver of global warming, involves the utilization of wood to establish carbon reservoirs, as depicted in Figure 1. In alignment with this ethos, ground improvement methodologies employing wood, which possesses resistance to biodegradation beneath the water table, have been conceived.

Conversely, the seismic event of the Great Tohoku Earthquake in 2011, particularly in Japan, induced widespread liquefaction occurrences across various regions, resulting in substantial damage to smaller-scale structures, notably single-family residences. Liquefaction mitigation techniques have not been

widely applied to residential buildings, underscoring the importance of investigating cost-effective strategies for liquefaction mitigation. Shallow ground improvement approaches, with a specific emphasis on the upper soil layers harboring a relatively thick liquefiable stratum, have been deemed as suitable measures for smaller residential edifices [1].

Presented as an approach that concurrently addresses concerns regarding carbon stock and liquefaction mitigation, a method involving the static installation of timber piles for soil densification and reinforcement has been introduced as shown in Figure 2. This conceptual framework, developed in recent years, seeks to alleviate excess pore water pressure and mitigate structural settlement [2].

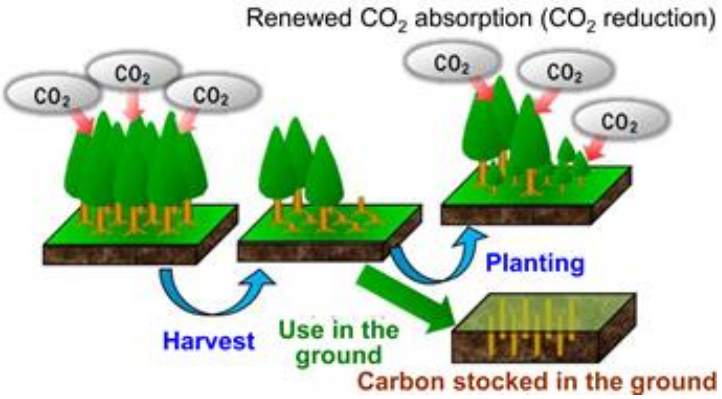

Figure 1. Effect of the log piling method on environment

LOG PILING FOR SHALLOW SOIL IMPROVEMENT IN LIQUEFACTION MITIGATION

Prior investigations into the utilization of log piles for liquefaction mitigation have already demonstrated their efficacy. In a 1-g shaking table experiment conducted by [3], it was emphasized that maintaining a center-to-center distance between log piles of 4 to 5 times their diameter yielded substantial liquefaction prevention effects, comparable to established densification methods. Further studies have also highlighted log piling's utility as a soil improvement technique near existing structures, showcasing its ability to reduce settlement and enhance the seismic resilience of buildings [4,5].

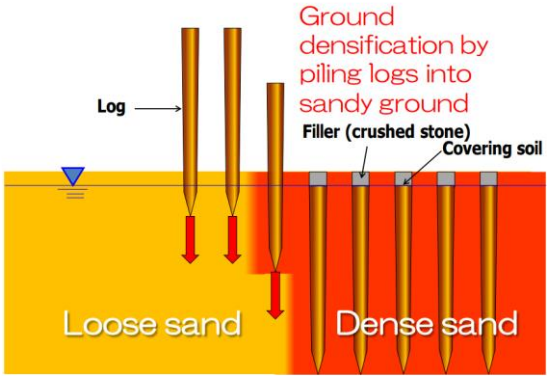

Figure 2. Installation of log piling by static pressing

Nevertheless, it is crucial to note that many previous studies assume the necessity of improving the entire liquefiable soil layer, which poses practical challenges when applying log piling as a liquefaction countermeasure for small residential structures. Additionally, numerous researchers have undertaken parametric studies based on 1-g shaking table model tests, investigating liquefaction mitigation through partial enhancement of soil conditions within the liquefiable layer. For instance, [6], utilized densification soil improvement techniques and explored parameters such as improvement width, structure width, and the ratio of width to height of the structure. Their findings indicate that

when the ratio of improved layer thickness to improved width exceeds 0.4, the ratio of liquefiable layer thickness to settlement tends to stabilize at an economically feasible level.

Similarly, [7], conducted a parametric analysis, considering structural dimensions, soil relative density, and liquefiable layer thickness. They observed that when the ratio of liquefiable layer thickness to the width of the structure exceeded 1.0, the ratio of liquefiable layer thickness to settlement remained below 5%. Thus, through 1-g shaking table model tests, the relationship between liquefaction-induced settlement and overall structural dimensions is often elucidated using various geometric ratios within the "liquefiable soil – improved zone – superstructure" system. However, there is currently a paucity of research exploring the concept of log piling as a liquefaction mitigation method at shallow depth. Against this backdrop, this study focuses on shallow soil improvement, offering a pragmatic and cost-effective solution for single-family residences situated atop thick liquefiable layers. The primary objective is to assess the efficacy of liquefaction mitigation through static log pile installation, accomplished through a series of 1-g shaking table model tests featuring variable parameters. Initially, small-scale experiments are conducted, varying improvement width, center-to-center pile distance, and the ratio of improvement depth to liquefiable layer thickness. Subsequently, medium-scale tests build upon these findings, exploring the influence of the absolute length of log piles while maintaining a consistent ratio of improvement depth to liquefiable layer thickness.

The central aim of this study is to establish practical thresholds and offer guidance to practitioners, facilitating the selection of an optimal configuration within the "liquefiable soil – improved zone – superstructure" system. This enables the effective adoption of log piling as a shallow soil improvement technique for liquefaction mitigation in the context of small residential constructions.

SOIL CONDITIONS IN EXPERIMENTS

In the presented study, Silica sand No. 7 has been chosen as the soil type due to its low resistance in terms of liquefaction potential. Key physical properties of this material, including particle density and maximum/minimum void ratio, have been determined through laboratory tests and are as follows: ρ_s=2.66 g/cm³, e_{min}=0.705 and e_{max}=1.178.

For the 1-g shaking table model tests, ground conditions with a relative density ranging from 40% to 50% (medium dense soil) have been selected.

SMALL-SCALE 1-G SHAKING TABLE TESTS

A small-scale rigid soil box, measuring 77.5 cm in width, 28 cm in depth, and 40 cm in height, has been employed for the experimental tests. To ensure appropriate scaling, the model has been downsized to 1/20th of its original dimensions. To account for the bending characteristics of the logs, we have implemented the similarity law introduced by [8]. For this study, PVC logs (sticks) were used instead of wooden ones. The house (superstructure) model's dimensions are 15 cm in width, 15 cm in depth, and 7.65 cm in height, with a base stress of 0.75 kPa. This base stress value, equivalent to 15 kPa in the prototype, realistically represents the scaled-down base stress encountered by small residential houses.

The primary objective of these experiments is to investigate the influence of three key parameters on liquefaction mitigation: 1) PVC log length (improved depth). 2) Improvement width. 3) Center-to-center spacing of the log piles. To streamline the testing process, the following approach was adopted: 1) A target relative density of 45% was set for the model soil. 2) Sand was initially introduced into a water-filled tank, and minor vibrations were applied to achieve the desired density up to a height of 30 cm. Subsequently, PVC logs were driven into the soil following a specific sequence for testing purposes. In subsequent trials, sand was not removed after the initial setup. Instead, high-pressure water was injected through valves to create loose ground conditions within the model. The water level was adjusted to match the ground level, and PVC logs were inserted for further experiments.

The experimental setup included various sensors, such as two laser displacement transducers positioned atop the superstructure model and an accelerometer mounted on the bottom surface of the shaking table. In Figure 3, Test 14 is depicted, Figure 4 shows an overview of the complete experimental set-up, while Figure 5 illustrates the initial state of the model and presents the input motion, involving 20 cycles at 5 Hz, with a gradual increase in excitation levels from 50 gal to 650 gal. Precise input accelerations were recorded using accelerometers strategically placed on the shaking table.

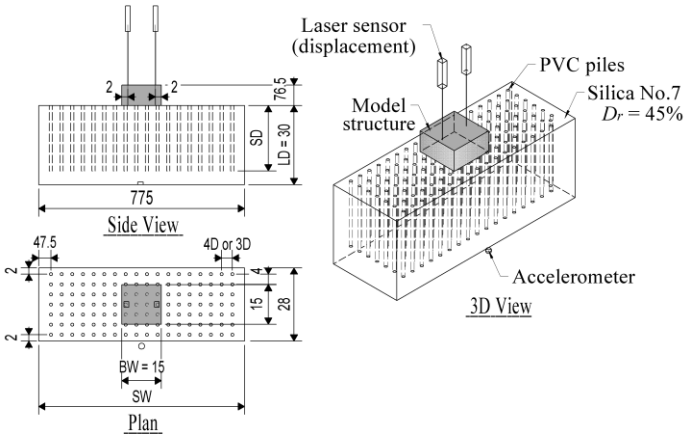

Figure 3. Side view, plan, and 3D view of the model (Test 14)

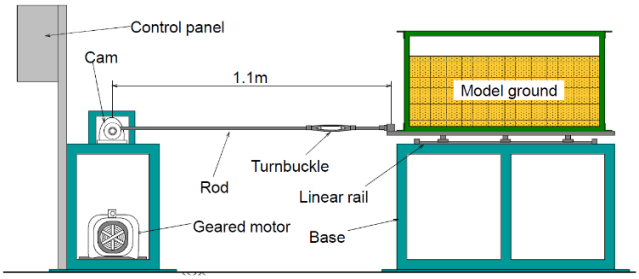

Figure 4. Small-scale 1-g shaking table set-up

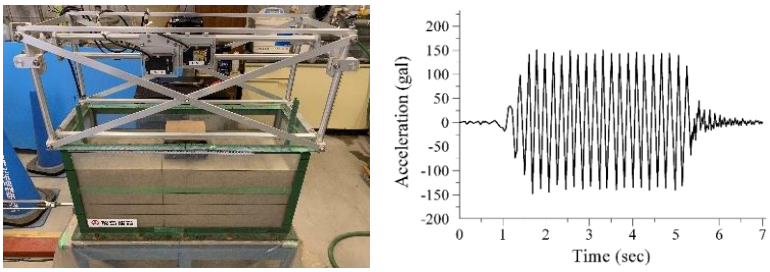

Figure 5. View of the test set-up (left) and input motion (right)

Figure 6 provides a detailed depiction of settlement measurements at each corner of the model following each step of excitation. Total settlement was determined by averaging the settlements recorded by the two laser displacement transducers. Penetration settlement of the model house was defined as the difference between the superstructure's settlement and the soil settlement.

Table 1 provides a comprehensive overview of the experimental setup, encompassing a total of sixteen cases. These cases scrutinize three critical parameters: 1) Improved depth. 2) Improvement width. 3)

Center-to-center spacing of the log piles. The log pile lengths utilized in the experiments are 25 cm, 17.5 cm, and 10 cm, corresponding to a liquefiable soil layer thickness (LD) of 30 cm. The log spacing

configurations are either 4D (equivalent to four times the log pile's diameter) or 3D (three times the log pile's diameter). In all cases, the log piles boast a uniform 1 cm diameter (*D*).

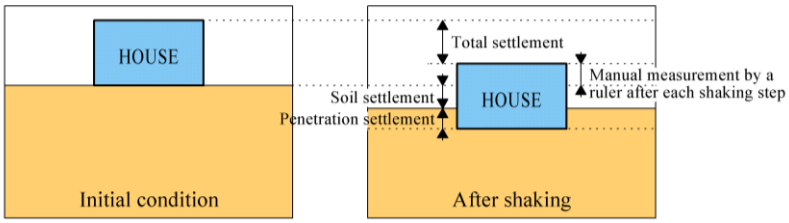

Figure 6. Definition for total settlement and penetration settlement

The chosen improvement widths encompass 13 cm, 37 cm, and 69 cm for scenarios with 4D spacing, and 16 cm and 40 cm for those with 3D spacing. To provide a comprehensive visual representation of the test conditions, both top-view and side-view depictions are presented in Figure 7 and Figure 8, respectively.

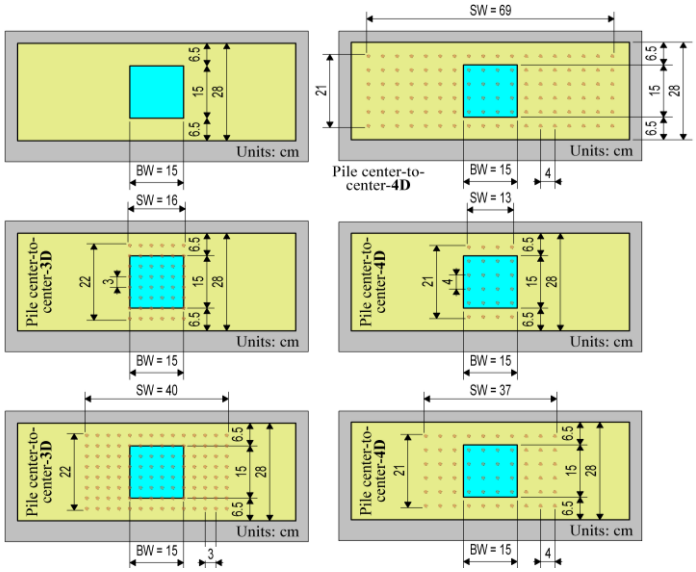

Figure 7. Top view of tests conditions (small-scale 1-g model tests)

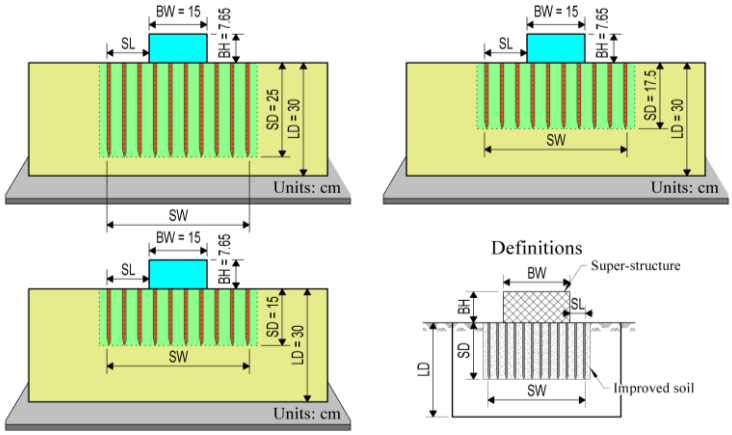

Figure 8. Side view of test conditions (small-scale 1-g model tests) and basic geometrical definitions

The presented research investigation delves deeply into the nuanced effects of varying improvement widths and center-to-center distances among log piles on both the overall and penetration settlements experienced by the superstructure. This comprehensive analysis encompasses diverse log pile lengths, each corresponding to distinct improved depths (SD) relative to the thickness of the liquefiable soil layer (LD) at ratios of 0.83, 0.58, and 0.33.

Table 1. Test conditions for small-scale 1-g shaking table tests

Test ID	Pile center-to-center distance	SW: Improvement width (cm)	SD: Improvement depth (cm)
Test 01	No improvement		
Test 02	4D (four times pile diameter)	13	25
Test 05		37	25
Test 06		13	17.5
Test 09		37	17.5
Test 10		13	10
Test 13		37	10
Test 14		69	25
Test 15		69	17.5
Test 16		69	10
Test 17	3D (three times pile diameter)	16	25
Test 18		40	25
Test 19		16	17.5
Test 20		40	17.5
Test 21		16	10
Test 22		40	10

Figure 9 serves as a visual representation of the intricate interplay between input acceleration and the resulting total settlement, meticulously captured through precision laser displacement sensors. In parallel, it provides a graphical depiction of the relationship between input acceleration and penetration settlement, discerned from averaged measurements obtained from the four corners of the model structure.

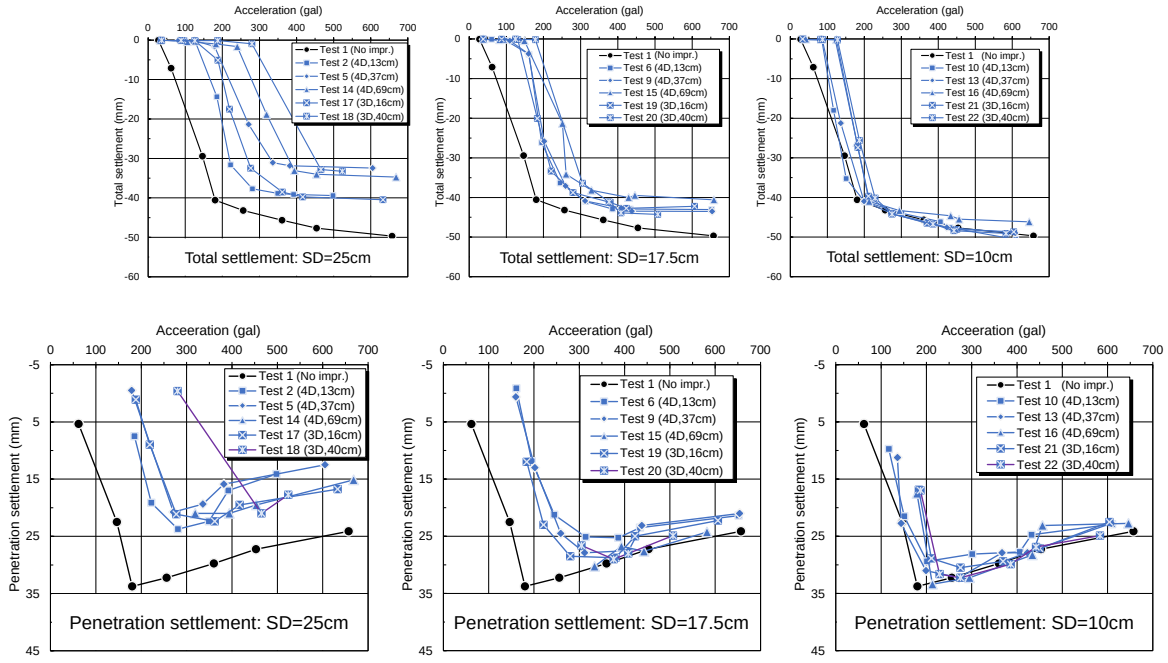

Figure 9. Cumulative settlement with acceleration increase – influence of the improved width and logs center-to-center distance

Specifically, when examining scenarios featuring an improved depth of 25 cm, a meticulous comparison has been undertaken among cases with identical log spacing but varying improvement widths. Notably, in instances characterized by 4D log spacing, a clear trend emerges: wider improvement widths yield substantially more pronounced reductions in settlement, while smaller log spacings accentuate this effect. Subsequent scrutiny has shifted to cases exhibiting similar improvement widths but divergent log spacings. Notably, within the context of 3D log spacing, both Test 2 and Test 17 initiate settlement responses at the same critical acceleration level (190 gal).

However, Test 2 exhibits more considerable settlement. A comparable pattern is observed in the case of Test 5 and Test 18. Broadly speaking, the configuration involving 3D log spacing tends to elicit a more pronounced improvement effect, particularly when coupled with larger improvement widths.

Furthermore, cases characterized by an improvement depth of 17.5 cm exhibit analogous trends concerning improvement width and log spacing. Similarly, instances marked by an improvement layer thickness of 10 cm, featuring 3D log spacing, generally produce marginally superior results. It is important to note that penetration settlement tends to decrease as total settlement escalates. This phenomenon can be attributed to the ongoing ground settlement process and the buoyancy effect exerted by the log piles on the superstructure, highlighting the multifaceted dynamics at play in liquefaction mitigation scenarios.

The study's findings shed light on how variations in log pile lengths (SD) exert influence over both the total and penetration settlements of the model structure, while keeping improvement widths and log spacings constant. To investigate these effects, log pile lengths corresponding to improved depth to liquefiable soil layer thickness (LD) ratios of 0.83, 0.58, and 0.33 have been considered for both 4D and 3D log spacing configurations. Specifically, for 4D log spacing, improvement width (SW) to house width (BW) ratios of 0.87 and 2.47 have been utilized, while for 3D log spacing, the ratios are 1.07 and 2.67. In Figure 10, the intricate relationships between acceleration and cumulative settlement are illustrated for three distinct improvement widths under 4D log spacing conditions. When the improvement width is set at 13 cm, Tests 2 and 6 exhibit similar settlement trends until total settlement stabilizes beyond 300 gal. Specifically, Test 2 reaches a settlement of 31.61 mm at 220 gal, Test 6 records 36.35 mm at 240 gal, and Test 10 achieves 41.03 mm at 200 gal. In contrast, with an improvement width of 37 cm, Test 5 shows 21.35 mm settlement at 270 gal, Test 9 registers 37.1 mm, and Test 13 observes 43.97 mm. It is evident that larger improvement widths result in more substantial reductions in total settlement, particularly when accompanied by greater improvement depth. Nevertheless, for an improvement width of 13 cm, the disparity in settlement between improvement depths of 25 cm and 17.5 cm is minimal. Figure 10 further elucidates the connection between acceleration and cumulative settlement for two different improvement widths under 3D log spacing. With a 16 cm width, Test 17 exhibits 5.11 mm settlement at 180 gal, Test 19 records 20.06 mm, and Test 21 observes 27.42 mm. In contrast, for a 40 cm width, Test 18 shows 0.94 mm settlement at 280 gal, Test 20 documents 23.5 mm, and Test 22 notes 44.18 mm. Larger improvement widths exhibit a more pronounced impact on total settlement, with the role of improvement depth becoming increasingly significant within this context.

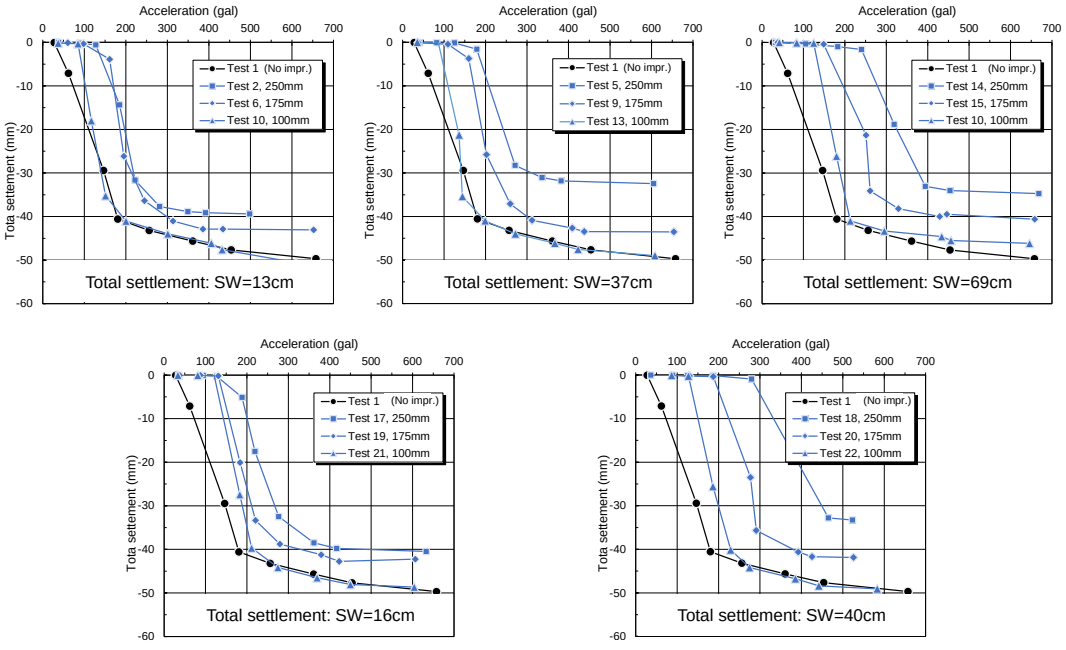

Figure 10. Cumulative settlement with acceleration increase – influence of the improved depth

The presented part of the study conducts a comparative analysis with prior research undertaken by [6], as illustrated in Figure 11. This comparison focuses on assessing how improvement width (SW) and depth (SD) impact the total settlement during seismic events. The study utilizes crucial parameters, including the ratio of improvement width to structure width (SW/BW) and the ratio of total settlement to the thickness of the liquefiable layer.

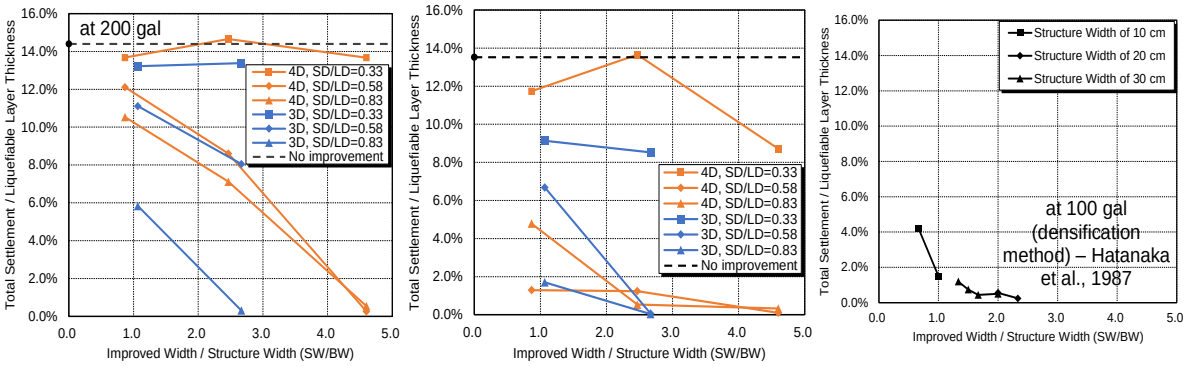

Figure 11. Effect of the log piling method on environment

The results shed light on the influence of various factors. For instance, when the improvement depth is set at 10 cm, which corresponds to an SD/LD ratio of 0.33, augmenting the improvement width has a relatively minor impact on the total settlement. In contrast, for depths of 17.5 cm and 25 cm (corresponding to SD/LD ratios of 0.58 and 0.83, respectively), wider improvement widths exhibit a notable reduction in settlement. An interesting observation is that at an improvement depth of 17.5 cm (SD/LD ratio of 0.58), the significance of log spacing diminishes when SW/BW exceeds 1.6. Furthermore, the findings suggest a broader trend: regardless of the specific improvement method employed, there is a noticeable stabilization of the total settlement to liquefiable layer thickness (LD) ratio when SW/BW surpasses the 1.6 threshold. This implies that increasing the improvement width beyond this point has a diminishing effect on settlement, particularly for a given level of acceleration.

In summary, for seismic events within the 150~200 gal range, the study identifies key parameters that effectively contribute to settlement reduction. These parameters include a log spacing of approximately 3D, an SW/BW ratio of 1.6, and an SD/LD ratio of 0.58.

MEDIUM-SCALE 1-G SHAKING TABLE TESTS

Silica sand No. 7 was intricately poured into a laminar soil box characterized by internal dimensions of 100 cm in width, 40 cm in depth, and 70 cm in height, as visually represented in Figure 12. The experimental conditions meticulously replicated those of the small-scale 1-g model tests. These conditions included maintaining a model-to-prototype ratio of 1/20, employing PVC piles (sticks) in lieu of wooden piles, adopting a pile diameter (D) of 1 cm, maintaining a structural width to height ratio (BW/BH) of 2.0, and applying a base stress of 0.75 kPa.

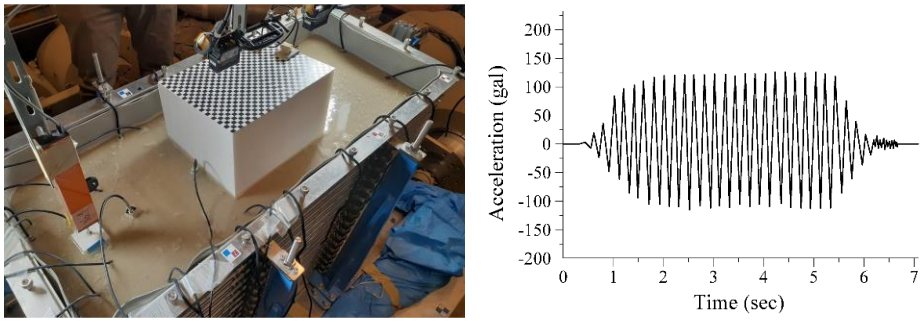

Figure 12. Model view (left) and input motion (right)

Table 2 provides a succinct overview of the five experimental cases, encompassing two cases without any improvement, distinguished by variations in liquefiable layer thickness (LD), and three cases implementing log pile densification improvement. Across all these scenarios, the ratio of improved depth to liquefiable layer thickness (SD/LD) is consistently maintained at 0.58, while preserving an improvement width to structure width ratio of 1.6. Moreover, the center-to-center distance between log piles is uniformly set at 3D for all cases. The primary focus of this series of tests revolves around emphasizing the absolute value of log pile length, or the improvement depth. Figure 13 offers a comprehensive side view of the test conditions across all experiments, clearly illustrating the placement of pore-water pressure transducers and accelerometers utilized in this study.

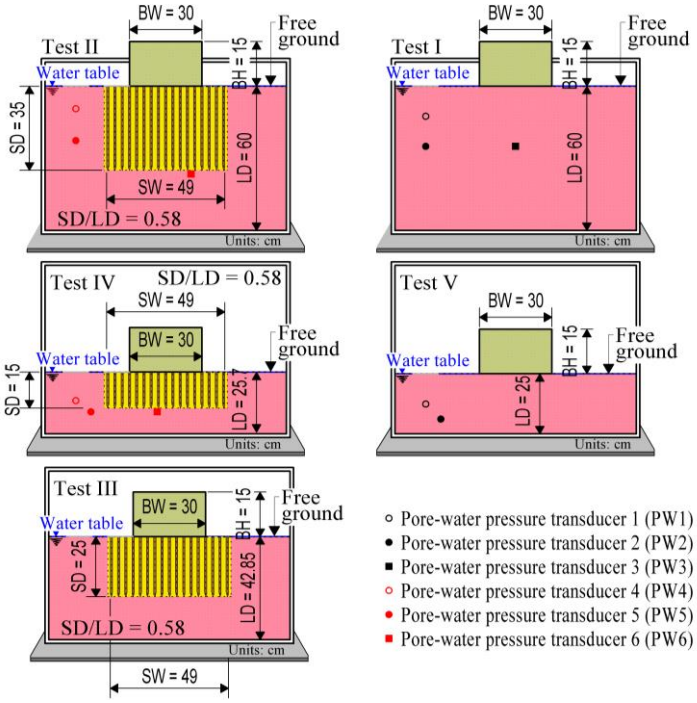

Figure 13. Side view of test conditions (medium-scale 1-g model tests)

Table 2. Test conditions for medium-scale 1-g shaking table tests

Test ID	SD: Improvement depth (cm)	LD: Liquefiable layer thickness (cm)	SD/LD Ratio
Test I	No improvement	60	-
Test II	35	60	0.58
Test III	25	42.85	
Test IV	15	25.7	
Test V	No improvement	25	-

Figure 14 illustrates the correlation between excess pore water pressure (PWP) ratio and cumulative penetration settlement. Comparing Test I and Test II, it is evident that both of them exhibit settlement within a certain PWP ratio range.

Similarly, Test II shows settlement within a similar range at equivalent PWP ratio levels, indicating the effectiveness of measures in Test II in reducing settlement compared to Test I. Such trend is also observed in the comparison of Test V and Test IV. Additionally, when comparing Test II and Test IV, Test II's measures achieve a more significant favorable effect.

Moreover, a comparative analysis of the acceleration responses in Test I and Test II is presented in Figure 15. The horizontal axis represents input acceleration, while the vertical axis displays the values measured by each accelerometer. First, the acceleration response at the top of the structure is examined. In Test I, it can be observed that after the liquefaction of the ground directly beneath the structure, the amplification in response decreases. Conversely, in Test II, although the amplification in

response decreases in the free ground following liquefaction, it remains unchanged at the top of the structure. From these observations, it can be inferred that after liquefaction, the top of the structure in Test I experiences a reduction in response amplification, while Test II does not. This suggests that the stiffness of the ground in the improved area may have been maintained even after an increase in excess pore-water pressure. Furthermore, when comparing the free ground in Test I and Test II, it is evident that, for similar input motion, Test II exhibits a higher amplification in response. This suggests that the ground surrounding the improved zone may have undergone densification or reinforcing due to the presence of the piles. The acceleration response trends of the Test V and Test IV are similar, which means that liquefaction countermeasures in Test IV were not effective enough to maintain soil's stiffness during the shaking.

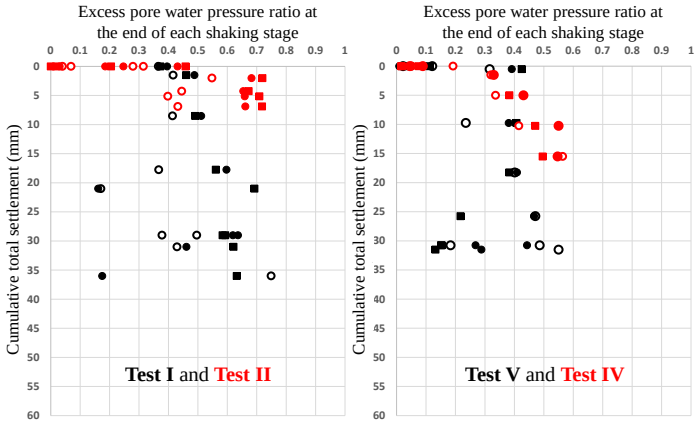

Figure 14. Relationship between excess pore water pressure ratio and cumulative total settlement at the end of each shaking stage

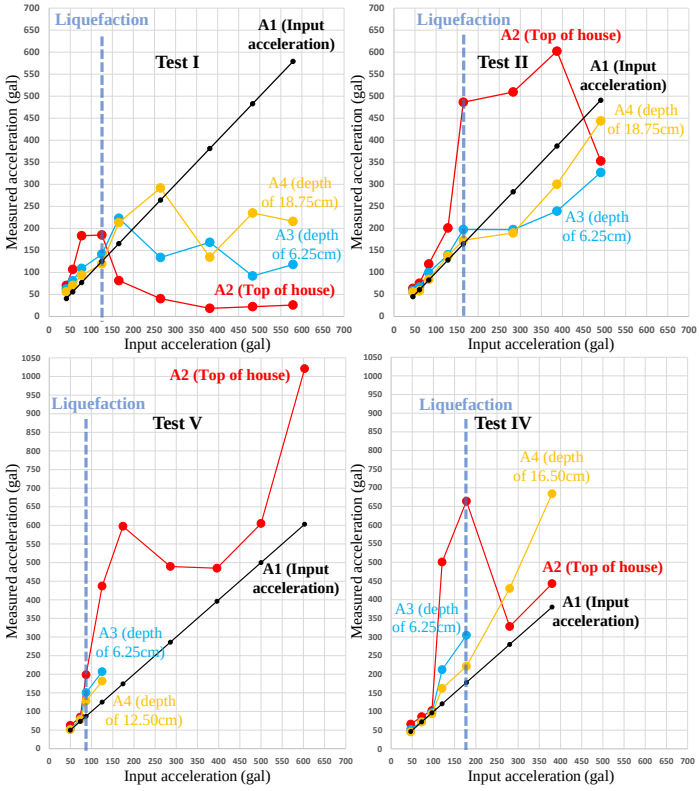

Figure 15. Comparison of acceleration response to input acceleration

The angles of some piles after their excavation are illustrated in Figure 16. The horizontal axis represents the position of the piles, while the vertical axis represents the tilt angles. Since the piles were manually driven, they may not be perfectly vertical, and there should be some degree of

inclination before shaking was applied. Therefore, the evaluation focuses on the trend in angle magnitude rather than the exact angle values. Test II's angle data, depicted on the left side of Figures 16, indicates an absence of any significant angle trend across the piles. Test IV's angle data, represented in the right side of Figures 16, exhibits a trend with the left part of the graph showing larger negative angles and the right half of the graph showing larger positive angles. Middle part of Figure 16 schematically illustrates such behaviour.

Results show minimal lateral spreading in Test II, suggesting effective shear deformation restraint by the piles in the improved soil, while Test IV is associated with a failure mechanism (lateral spreading due to liquefaction).

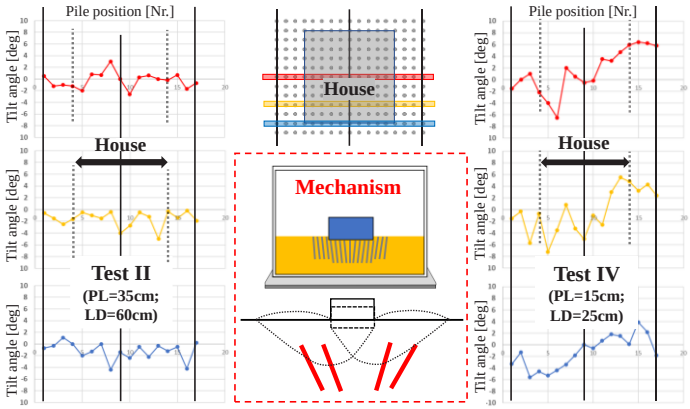

Figure 16. Piles tilt trend and detection of failure mechanism

Figure 17 offers a comprehensive summary of the results obtained from the medium-scale 1-g shaking table tests, outlining key trends concerning both penetration settlement and total settlement of the structure. In scenarios where no mitigation measures were applied, specifically Test I and Test V, it is evident that Test I, characterized by a greater liquefiable layer thickness (LD), experiences a correspondingly larger penetration settlement. However, when these cases are compared to scenarios involving the implementation of piles, such as Test II, Test III, and Test IV, a significant pattern emerges.

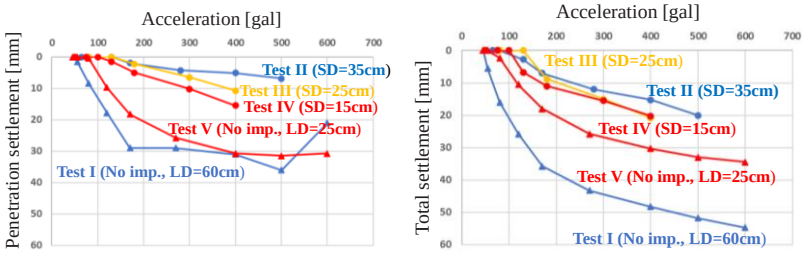

Figure 17. Acceleration versus penetration settlement/total settlement

Test II, featuring the longest pile length and LD, exhibits the smallest magnitude of penetration settlement. Conversely, Test IV, characterized by the smallest SD and LD values, displays the most substantial penetration settlement. Additionally, similar trends are observed when analyzing total settlement.

UNDRAINED CYCLIC TORSIONAL SHEAR TESTS

Data from undrained cyclic torsional tests (Figure 18 – right) played a pivotal role in calibrating the constitutive model (PM4Sand) employed for the numerical study. The tested material aligned with that utilized in the 1-g shaking table tests – Silica sand No. 7 at a relative density of 50%.

The torsional shear apparatus (Figure 18 – left) featuring hollow cylindrical specimens is acknowledged as a valuable tool for accurately assessing the soil response to liquefaction [9]. Notably,

it allows the replication of simple shear conditions, which closely resemble the stress state experienced in the field during earthquakes. To prepare the specimens, four medium-sized hollow cylindrical specimens with dimensions of 100 mm in outer diameter, 60 mm in inner diameter, and 200 mm in height were created using the air pluviation method. To achieve specimens with highly uniform density, the falling height was meticulously maintained constant throughout the pluviation process. A high degree of saturation was accomplished (with Skempton's *B*-values exceeding 0.96) by continuously circulating de-aired water into the specimens. The specimens have been isotropically consolidated by increasing the effective stress state, σ'_c, up to 100 kPa, with a back pressure, u_b, of 200 kPa. Subsequently, to emulate seismic conditions, a constant-amplitude undrained cyclic torsional shear stress, τ, was applied at a shear strain rate ranging from 0.25 to 1.0% per minute.

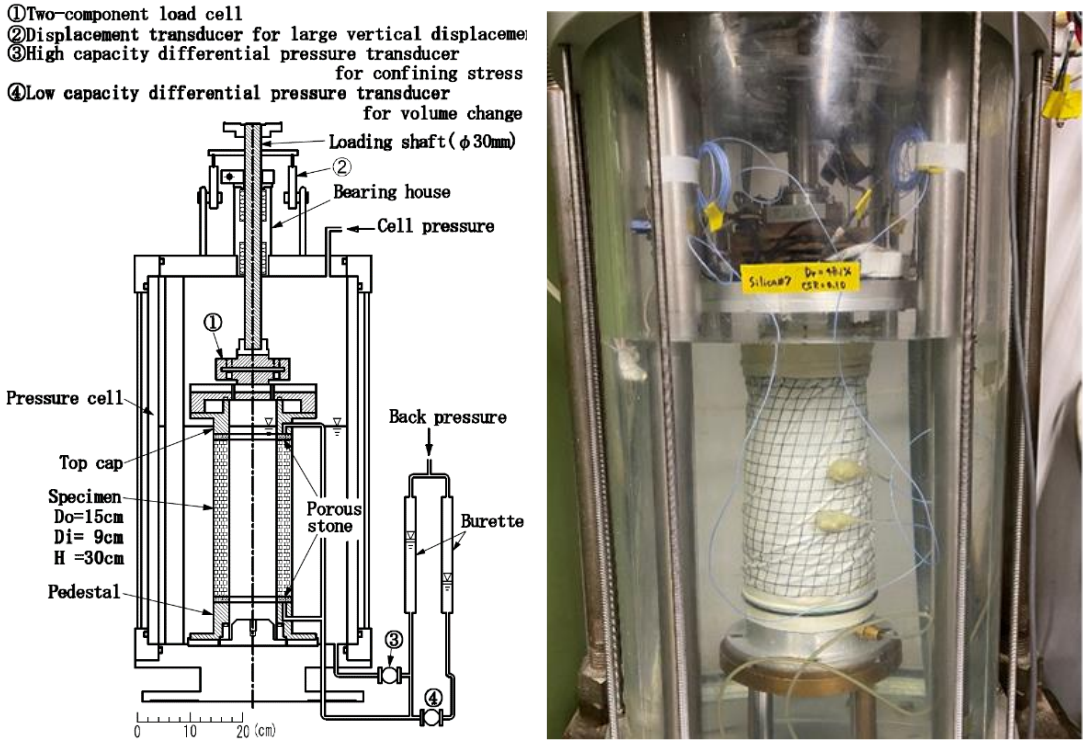

Figure 18. Cyclic torsional tests: torsional shear apparatus scheme [9], left, and testing, right

Experiments were conducted at various cyclic stress ratios, CSR, defined as the cyclic stress, τ, divided by the effective stress, σ'_c, including values of 0.100, 0.150, 0.200, and 0.250. The objective was to establish the *CSR-N* relationship (where *N* represents the number of cycles required to generate a 7.5% double amplitude of shear strain) and to derive relationships for "cyclic shear stress – shear strain," pore water pressure buildup, and stress paths. Corresponding to a 7.5 magnitude earthquake, it was determined that 15 cycles were needed to reach liquefaction at a specific cyclic stress ratio. Therefore, the laboratory-derived cyclic resistance ratio, *CRR*, was determined using the *CSR-N* relationship for 15 cycles (Figure 20 – left), with *CRR* set at 0.172.

CALIBRATION OF PM4SAND CONSTITUTIVE MODEL

The numerical investigation in this study employs the PM4Sand constitutive model, renowned for its ability to effectively replicate sand material behavior under dynamic loading conditions. This model encompasses the intricate phenomena of pore pressure generation, liquefaction, and post-liquefaction responses, rendering it particularly appealing for industrial applications due to its parsimonious parameter set requiring calibration.

The PM4Sand model is rooted in the fundamental framework of stress-ratio controlled, critical state-compatible, bounding surface plasticity model for sands, as originally proposed by [10]. Subsequently, it has been adapted and configured in the context of plane stress conditions, as introduced by [11].

This adjustment facilitates its integration into 2D plane strain numerical models, where out-of-plane stress is omitted from the global finite element equations.

Model parameters are categorized into two groups, each serving specific purposes (detailed descriptions can be found in Table 3):

- A primary set comprising 4 parameters (D_{R0}, G_0, h_{p0}, and p_A), which hold paramount significance in the calibration process.
- A secondary set encompassing 9 parameters (e_{max}, e_{min}, n^b, n^d, ϕ_{cv}, ν, Q, R, and PostShake).

In this study, D_{R0}, e_{max}, and e_{min} have been determined based on outcomes from conventional laboratory tests that establish the physical characteristics of the soil. ϕ_{cv} has been established by referencing the critical line derived from stress paths, specifically cyclic torsional tests. G_0 has been derived from shear wave velocity (V_s) measurements employing bender elements conducted prior to the cyclic torsional tests. All other parameters, except for h_{p0}, have been utilized at their default values.

The calibration process for a relative density of 50% (representative of the non-improved zone) involves adjustments to h_{p0}, utilizing experimentally obtained data from cyclic torsional tests. The procedure can be summarized as follows:

- Set relative density, D_r, to 50%.
- Numerically simulate cyclic torsional tests across a range of cyclic stress ratios (*CSR*) corresponding to laboratory tests (0.100, 0.150, 0.200, and 0.250). Fit simulated stress paths, "cyclic shear stress - shear strain" relationships (see Figure 19), and the *CSR-N* relationship to match the experimentally obtained data (laboratory) – refer to Figure 20, left.

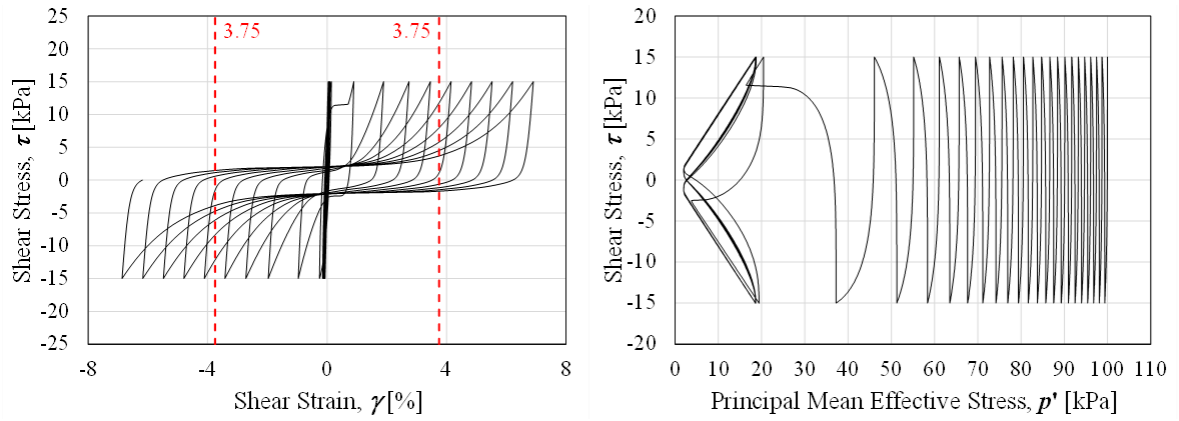

Figure 19. Numerically simulated cyclic torsional test: "cyclic shear stress – shear strain" relation, left, and stress path, right

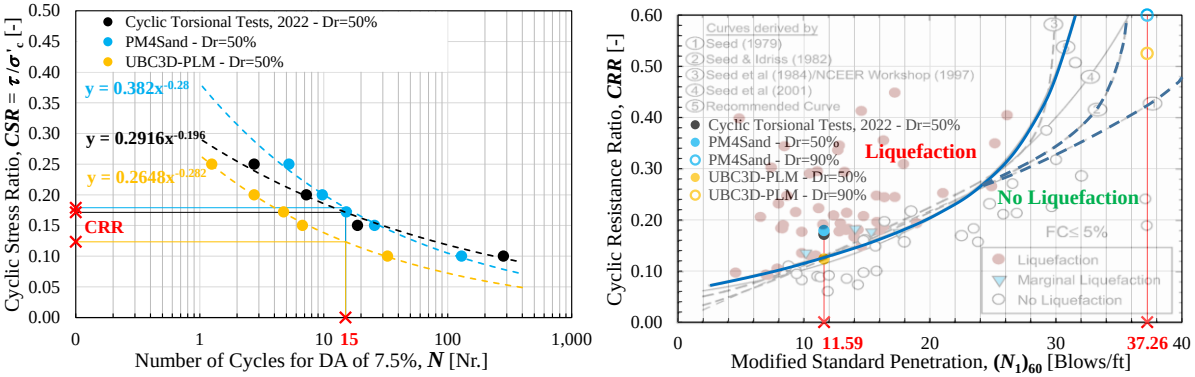

Figure 20. Comparison of experimentally and numerically obtained: CSR-N relationships, left, and CRR – plotted against a commonly used cyclic strength curve from the literature (Seed et al. 1985), right

- Define the cyclic resistance ratio (*CRR*) using the numerically and experimentally obtained *CSR-N* relationships for 15 cycles. Ensure that both *CRR* values closely align with each other

and compare them with commonly utilized cyclic strength curves from existing literature (accounting for the conversion of relative density, D_r, to energy-corrected SPT blow count, $(N_1)_{60}$, as shown in Figure 20, right).

- Given the absence of experimental data for a relative density, D_r, of 90% (representing the improved zone), a distinct procedure is adopted, with parameter variation exclusively focused on h_{p0}:
- Set relative density, D_r, to 90%.
- Convert D_r to $(N_1)_{60}$. Establish the *CRR* value corresponding to $(N_1)_{60}$ based on widely accepted cyclic strength curves from the literature.
- Simulate cyclic torsional shear tests and adjust the constitutive model parameters until the adopted *CRR* value aligns with the *CSR-N* relationship for 15 cycles.
- For reference, Table 3 provides the adopted values for all parameters used in the PM4Sand constitutive model formulation, accompanied by a concise overview of the calibration procedure.

Table 3. Summary of PM4Sand parameters – adopted values and calibration procedure

	Symbol	Adopted Value		Default Value	Unit	Description	Calibration Procedure
		D_{R0} = 50%	D_{R0} = 90%				
Primary Parameters	D_{R0}	0.50	0.90	-	[-]	Relative density	Lab data or D_{R0} = SQRT[$(N_1)_{60}$/46]
	G_0	625	1380	-	[-]	Shear modulus coefficient	$G_0 = [\rho (V_s)^2]/[p_A \times \text{SQRT}(p_{ref}/p_A)]$ or $G_0 = 167 \times \text{SQRT}[(N_1)_{60} + 2.5]$
	h_{p0}	0.545	0.425	-	[-]	Contraction rate parameter	Based on CRR-(N1)60 curve for M_w = 7.5 (or 15 uniform loading cycles - element tests) - fitting.
	p_A	101.3	101.3	101.3	[kN/m^2]	Atmospheric pres.	-
Secondary Parameters	e_{max}	1.225	1.225	0.8	[-]	Maximum void ratio	Basic physical parameters based on lab tests.
	e_{min}	0.727	0.727	0.5	[-]	Minimum void ratio	
	n^b	0.5	0.5	0.5	[-]	Bounding surface par.	-
	n^d	0.1	0.1	0.1	[-]	Dilatancy surface par.	-
	ϕ_{cv}	44.0	50.0	33	[^{o}]	Crit. state fric. angle	Basic strength parameters based on element tests.
	ν	0.3	0.3	0.3	[-]	Poisson's ratio	
	Q	10	10	10	[-]	Crictial state line parameters	-
	R	1.5	1.5	1.5	[-]		-
	PostShake	0	0	0	[-]	Post shake switch	PostShake switch (0 or 1) deactivates or activates the reduction of elastic stiffness in order to simulate the post-shaking reconsolidation. PostShake = 1 only after the end of strong shaking (two separate analysis phases).

COMPARISON BETWEEN PM4SAND AND UBC3D-PLM CONSTITUTIVE MODELS

The UBC Sand Constitutive Model (UBC3D-PLM in PLAXIS 2D library) is a widely used tool in geotechnical engineering, particularly for analyzing liquefaction phenomena in sandy soils under dynamic loading conditions, such as earthquakes. Developed at the University of British Columbia, this model is essential for simulating the complex behavior of sands, including pore pressure generation, liquefaction onset, and post-liquefaction responses. It requires calibration based on laboratory test data (procedure is given in Table 4) to accurately predict liquefaction potential, making it a valuable asset for assessing and mitigating liquefaction risks in engineering practice.

Utilizing the proposed calibration procedure for UBC3D-PLM, the selected parameters for this study are presented in Table 4. In order to facilitate a meaningful comparison between the outcomes of an undrained cyclic torsional shear test (specifically, with a *CSR* of 0.200) and those generated through numerical simulations employing two widely recognized and extensively employed constitutive

models, namely PM4Sand and UBC3D-PLM, particularly in the realm of liquefaction assessment, an illustrative representation is given in Figure 21.

Table 4. Summary of UBC3D-PLM parameters – adopted values and calibration procedure

	Symbol	Adopted Value		Default Value	Unit	Description	Calibration Procedure
		D_{R0} = 50%	D_{R0} = 90%				
Stiffness parameters	k^{*e}_B	732	977	-	[-]	Elastic bulk modulus fa	$k^{*e}_B = 0.7 \times k^{*e}_G$
	k^{*e}_G	1046	1395	-	[-]	Elastic shear modulus f	$k^{*e}_G = 21.7 \times 20 \times (N_1)_{60}^{0.3333}$
	k^{*p}_G	717	4723	-	[-]	Plastic shear modulus f	$k^{*p}_G = k^{*e}_G \times (N_1)_{60}^2 \times 0.003 + 100$
	me	0.65	0.50	0.50	[-]	Rate of stress-dependency of elastic bulk modulus	Step 1: Based on cyclic element tests - fitting of τ-γ and τ-p' curves.
	ne	0.65	0.50	0.50	[-]	Rate of stress-dependency of elastic shear modulus	
	np	0.55	0.40	0.40	[-]	Stress-dependency of plastic shear modulus	
Strength Parameters	p_{ref}	100	100	100	[kN/m^2]	Reference pressure	Basic strength parameters based on element tests.
	ϕ_{cv}	44.0	50.0	33	[^{o}]	Critical state friction an	
	c	0.0	0.0	0.0	[kN/m^2]	Cohesion	
	σ_t	0.0	0.0	0.0	[kN/m^2]	Tension cut-off and ten	
	ϕ_p	45.0	53.6	34.4	[^{o}]	Peak friction angle	$\varphi_p = \varphi_{cv} + (N_1)_{60}/10 + \max(0; [(N_1)_{60} - 15]/5)$
Advanced Parameters	$(N_1)_{60}$	14.03	33,24	-	[-]	Corrected SPT value	SPT data or $(N_1)_{60} = 46 \times (D_{R0})^2$
	R_f	0.74	0,65	0.90	[-]	Failure ratio	$R_f = 1.1 \times [(N_1)_{60}]^{-0.15}$
	f_{dens}	0.625	1.000	1.00	[-]	Densification factor	Step 2: Based on *CRR* -$(N_1)_{60}$ curve for M_w = 7.5 (or 15 uniform loading cycles - element tests) - fitting.
	f_{Epost}	0.200	1.000	-	[-]	Post-liquefaction factor	

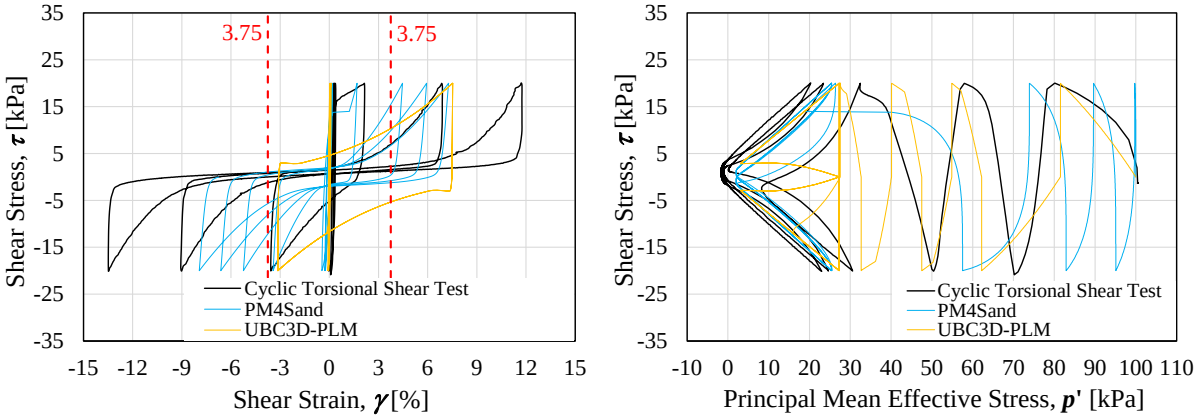

Figure 21. "Cyclic shear stress – shear strain" relation, left, and stress path, right – comparison between a cyclic torsional shear test and numerical simulations (PM4Sand and UBC3D-PLM)

Ultimately, PM4Sand has been chosen as the constitutive model for the presented FEM analysis, a preference commonly observed in engineering practice, particularly for conducting analyses related to liquefaction-induced settlement.

NUMERICAL MODEL

Figure 22 provides an illustrative depiction of the numerical model and the 1-g model setup. The numerical models, founded upon the Finite Element Method (FEM), have been meticulously developed using PLAXIS 2D software [12]. Three distinct models have been crafted to faithfully replicate the conditions observed in the 1-g model tests. The numerical models are inherently designed to mirror the experimental conditions. They encompass separate definitions for the improved zone, characterized by a relative density, D_r, of 90%, and the non-improved zone, featuring a relative density, D_r, of 50%. The log-piles, emulating the physical counterparts, are represented using embedded beam row elements. The structural representation aligns with the house configuration employed in the model tests, factoring in self-weight considerations (equivalent to a base stress of 15 kPa) and adhering to geometrical specifications.

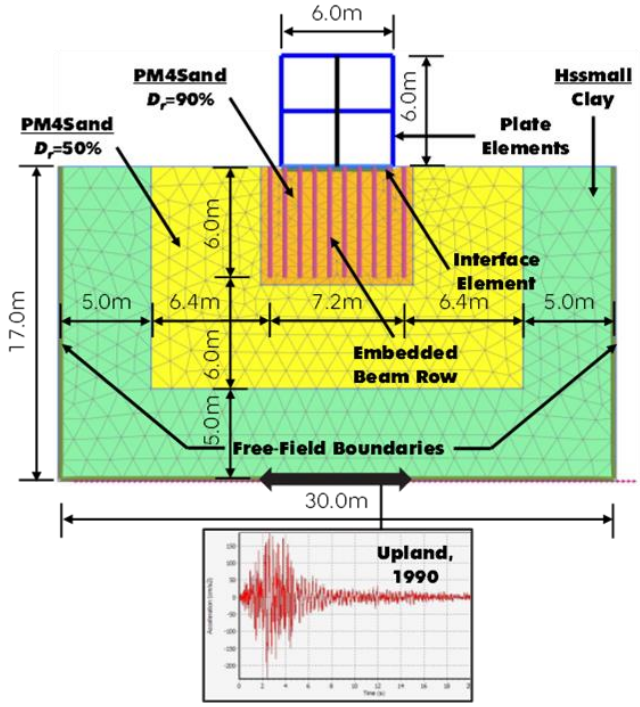

Figure 22. Overview of the numerical model

To account for interface dynamics between the soil and the superstructure, interface elements have been judiciously incorporated within the contact zone. Given the adoption of free-field boundary conditions, it is essential to acknowledge the potential for stress concentration within the region directly interfacing with the liquefiable material. Consequently, a drained zone consisting of non-liquefiable material (HS-Small Model) has been included as a supplementary feature around the liquefiable field. The time-history analysis leverages a representative accelerogram, sourced from the 1990 Upland earthquake records. To systematically scrutinize the system's response across varying acceleration levels, the accelerogram has been meticulously scaled for multiple iterations. It's important to acknowledge that while the physical and numerical models endeavor to capture similar phenomena, direct comparisons are somewhat limited due to inherent differences in scale and input motion between the two approaches.

FEM ANALYSIS RESULTS

Figure 23 and Figure 24 present notable findings from the numerical simulations conducted at an approximate ground acceleration of 140 gal.

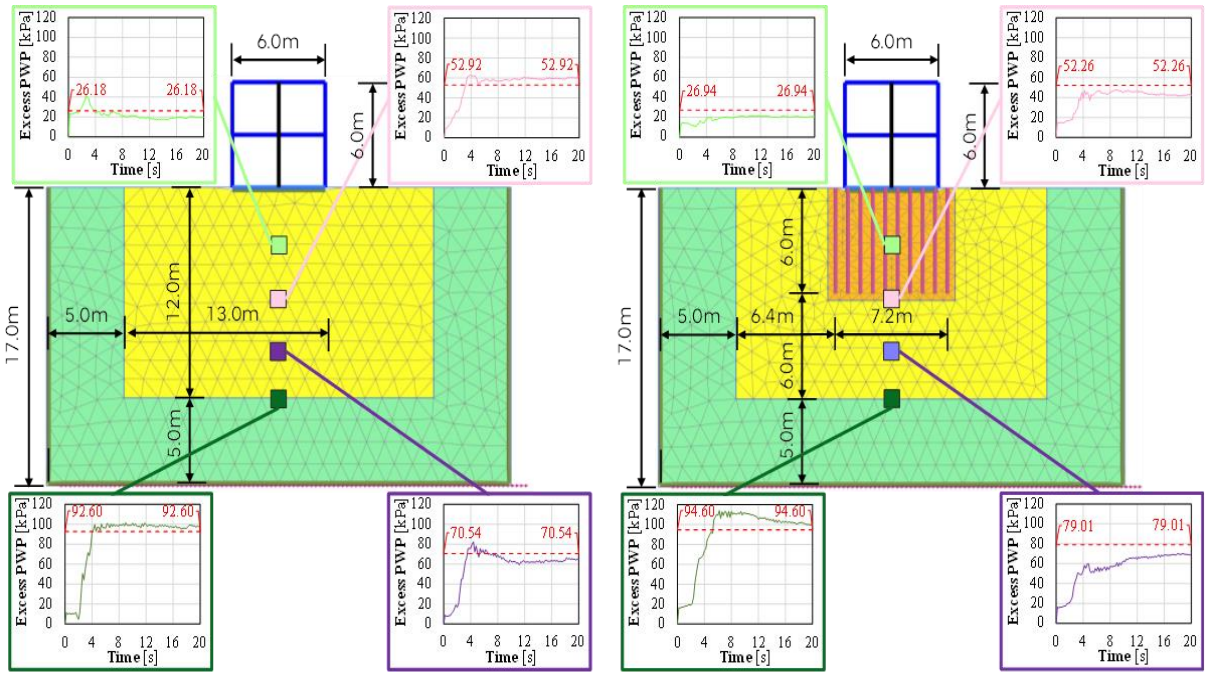

Figure 23. 140 gal: Excess pore-water pressure time history in unimproved case (left) and improved case – piles below and around the structure (right)

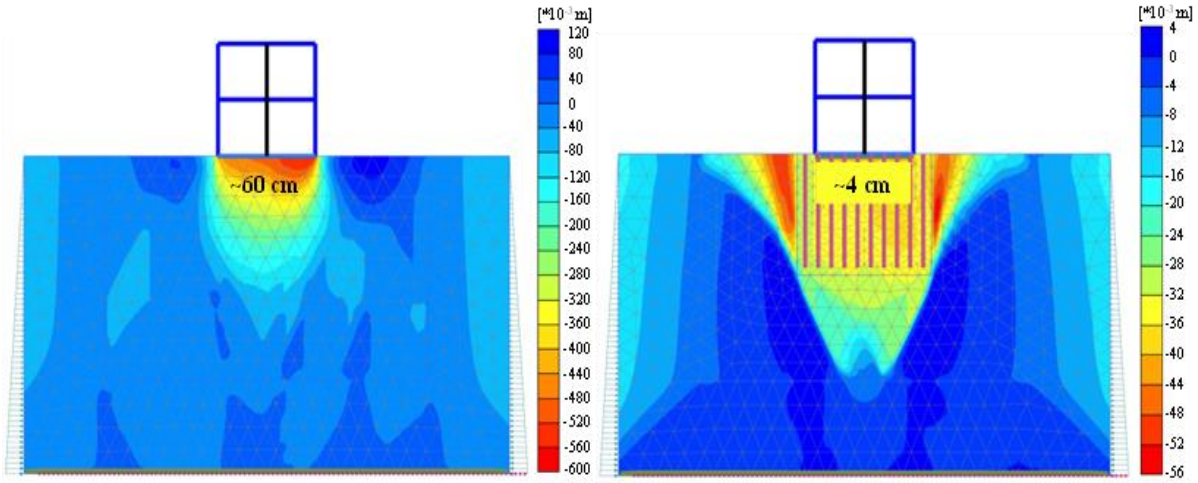

Figure 24. 140 gal: Vertical deformation (liquefaction-induced settlement) of unimproved case (left) and improved case – piles below and around the structure (right)

The analysis of excess pore-water pressure build-up highlights a significant contrast between the non-improved and improved cases. In the former, the entire sand layer experiences liquefaction. Conversely, the improved case demonstrates a more favorable response, with liquefaction observed solely at a depth of 12 meters. In other zones, the ratio of pore-water pressure to effective stress remains below 1.0. This comparison strongly suggests that shallow ground improvement through log-pile installation could positively influence the behavior of the "superstructure – foundation – soil" system, potentially serving as an effective countermeasure against liquefaction. Furthermore, the impact of improvement becomes more evident when assessing the settlement of the superstructure. At an acceleration of approximately 140 gal, the improved case exhibits settlement more than five times smaller than the non-improved case – specifically, 120 mm compared to 618 mm. Liquefaction-induced settlement serves as a pivotal metric for quantifying the effectiveness of mitigation measures.

Figure 25 (left) provides a summarized representation of normalized total settlements derived from the numerical analysis. A comparison with the 1-g shaking table test study by [13], reveals a noteworthy

alignment in trends between both approaches. At relatively low accelerations of 80 gal, the non-improved case experiences significant settlement of the superstructure, while the two improved cases show considerable reductions in vertical displacements. This trend becomes even more pronounced with increasing acceleration. The two improved cases, involving improvement beneath the superstructure and improvement encompassing both beneath and around it, exhibit similar responses of the "superstructure – foundation – soil" system.

However, differences in response become apparent after approximately 300 gal, emphasizing the influence of additional improvement width around the house. This reaffirms the recommendations from prior studies [6,14,15] regarding the inclusion of such an additional treatment zone. Figure 25 (right) supplements this by summarizing the collective insights of other authors [16] concerning the significance of the improvement thickness (utilizing various liquefaction mitigation techniques) in relation to the total liquifiable layer thickness ratio. The graph clearly demonstrates that a ratio exceeding 0.5 significantly reduces liquefaction-induced settlement – a conclusion reinforced by the results of the current study.

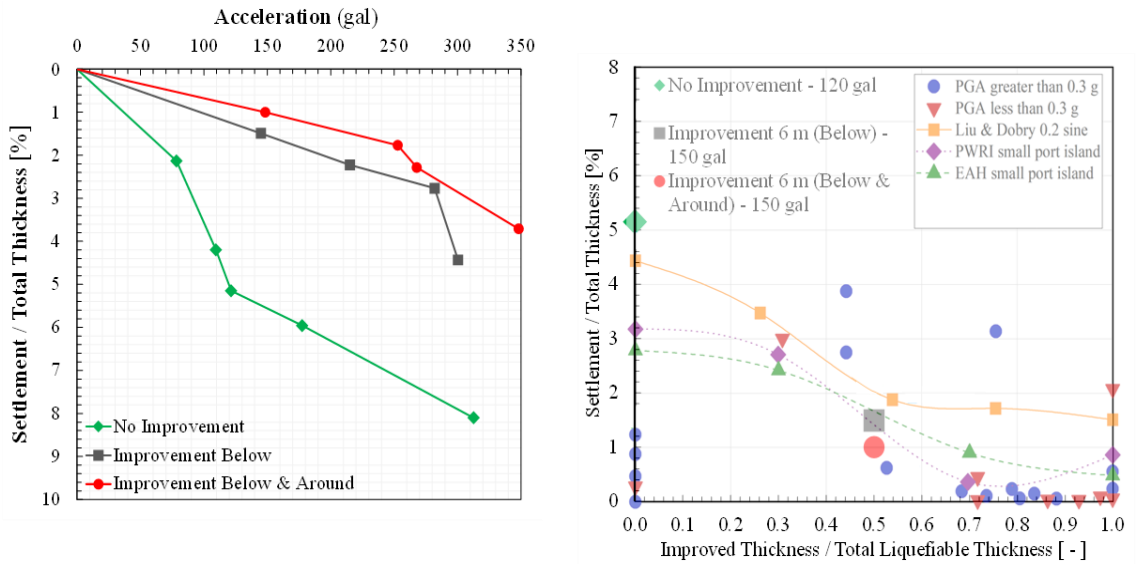

Figure 25. Normalized total settlement against acceleration, left, and countermeasure effect from this study and previous studies (New Zealand Geotechnical Society, 2017), right

CONCLUSIONS

The research presented in this paper highlights the effectiveness of the log piling method as a viable solution for mitigating soil liquefaction, especially in shallow ground improvement scenarios. By increasing soil density and providing reinforcement, log piling plays a crucial role in preventing liquefaction and reducing structural damage. The study initially focused on determining the impact of three critical factors – depth of improvement, width of improvement, and spacing between log piles – on the total and penetration settlements of structures. These evaluations were carried out using 1-g shaking table tests in a small-scale rigid soil box, revealing that wider improvement areas and closer pile spacing significantly influence settlements caused by liquefaction.

Key findings of this research include insights into mitigating liquefaction during seismic activities within the 150-200 gal range. The study identified three vital parameters for minimizing liquefaction effects: 1) The optimal center-to-center spacing of log piles, found to be about three times their diameter. 2) The ratio of improvement width to the structure's width, which proved most effective when exceeding 1.6. 3).

The ratio of the thickness of the improved layer to the thickness of the liquefiable layer, with maximum effectiveness around 0.58. Building on these findings, the research progressed to a second

phase involving medium-scale 1-g shaking table experiments in a laminar soil box, focusing on the impact of log pile length (improved depth). The results indicated that longer piles are more effective in reducing excess pore water pressure and settlement from liquefaction, maintaining a constant ratio of improved depth to liquefiable layer thickness. Furthermore, the study highlighted the importance of utilizing data from laboratory element tests, like cyclic torsional shear tests, for calibrating constitutive models.

Comparing results from 1-g shaking table tests with numerical finite element method (FEM) simulations showed consistent trends, affirming the positive impact of log piling even when treating a small portion of the liquefiable layer. Overall, the findings provide crucial guidance for optimizing the use of log-based techniques in liquefaction mitigation for engineering applications.

ACKNOWLEDGEMENTS

This study has been supported by Scientific Research Grant PE20027 provided by Japan Society for the Promotion of Science (JSPS). The authors extend their sincere gratitude to Tobishima Corporation for their unwavering support throughout the entire reserach process.

(Received May 2022, accepted June 2022)

REFERENCES

[1] Tani, K., Kiyota, T., Matsushita, K., Hashimoto., Yamamoto, A., Takeuchi, H., Noda, T., Kiku, H. and Obayashi, J. (2015). Liquefaction countermeasures by shallow ground improvement for houses and their cost analysis. *Soil Dynamics and Earthquake Engineering*, No, 79, pp. 401-414.

[2] Riaz, S. Numata, A., Mimura, K., Ikeda, H. and Hori, T. (2014). The Effect of Log Piling on Liquefaction. *Journal of Japan Society of Civil Engineers*, Vol. 2, pp.144-158.

[3] Numata, A., Murata, T., Riaz, S., Mimura, K. and Hara, T. (2015). Effect of log piling method for liquefaction countermeasures by large-scale shaking table test, *Proceedings of the Japan Society of Civil Engineers (Structural and Earthquake Engineering)*, Vol. 71, No. 4 (Earthquake Engineering Proceedings Vol. 34), pp. 274-283 (in Japanese).

[4] Miwa, S., Yoshida, M., Murata, T. and Numata, A. (2016): Shaking table tests and numerical analysis on log piling as a liquefaction countermeasure for existing houses, *Proceedings of the Japan Society of Civil Engineers A1 (Structural and Earthquake Engineering)*, Vol. 72, No. 4 (Earthquake Engineering Proceedings Vol. 35), pp. 117-128 (in Japanese).

[5] Serikawa, Y., Yoshida, M. and Miyajima, M. (2016): Study on liquefaction countermeasure technique by log piling for existing residential houses, *Proceedings of the Japan Society of Civil Engineers A1 (Structural and Earthquake Engineering)*, Vol. 72, No. 4 (Earthquake Engineering Proceedings Vol. 35), pp. 489-495 (in Japanese).

[6] Hatanaka, M., Suzuki, Y., Miyaki, M. and Tsukuni, S. (1987). Some Factors Affecting the Settlement of Structures Due to Sand Liquefaction in Shaking Table Tests. *Soils and Foundations*. Vol. 27, Issue 1, pp 94-101.

[7] Yoshimi, Y., and Tokimatsu, K. (1977). Settlement of Buildings on Saturated Sand During Earthquakes, *Soils and Foundations*, Vol. 17, No. 1, pp. 23–38.

[8] Iai, S. (1989). Similitude for Shaking Table Tests on Soil-Structure-Fluid Model in 1g Gravitational Field. *Soils and Foundations*, Vol. 29, Issue 1, pp. 105-118.

[9] Kiyota, T., Koseki, J. and T. Sato. (2010). Comparison of liquefaction-induced ground deformation between results from undrained cyclic torsional shear tests and observations form previous model tests and case studies. *Soils and Foundations*. Vol. 50, pp 421-429.

[10] Dafalias, Y.F. and Manzari, M.T. (2004). Simple plasticity sand model accounting for fabric change effects. *Journal of Engineering Mechanics*, ASCE, 130(6), pp. 622-634.

[11] Boulanger, R.W. and Ziotopoulou, K. (2017). PM4Sand (Version 3.1): A sand plasticity model for earthquake engineering applications. *Report No. UCD/CGM-17/01*, Center for Geotechnical Modeling, Department of Civil and Environmental Engineering, University of California, Davis, CA.

[12] PLAXIS (2019). *PLAXIS 2D Reference Manual*. Bentley Systems International Limited, Dublin.

[13] Osawa, S., Milev, N., Kiyota, T., Shiga, M., Ito, R., Katagiri, T., Numata, A. (2023). Shaking table tests to evaluate liquefaction mitigation effect of log piling technique in application to shallow ground improvement. *Proc. Of 17th Danube – European Conference on Geotechnical Engineering (17DECGE)*.

[14] Fire Defence Agency (1974). *Notification specifying detailed provisions of technical criteria for regulating dangerous articles* (in Japanese).

[15] Tsuchida, H., Iai, S. and Kurata, E. (1976). On zone of soil property improvement of soils. *Proc. of 14th Meeting of Earthquake Engineering*, pp. 9-12 (in Japanese).

[16] New Zealand Geotechnical Society. (2017). *Earthquake geotechnical engineering practice – Module 5: Ground improvement of soils prone to liquefaction*.